Setup for in situ surface investigations of the liquid/glass transition with (coherent) x rays

Tilo Seydel, Anders Madsen, Michael Sprung, Metin Tolan, Gerhard Grübel, Werner Press

A setup for in-situ surface investigations of the liquid/glass transition with (coherent) x-rays

Tilo Seydel[(1)(*)], Anders Madsen[(2)], Michael Sprung[(3)],
Metin Tolan[(3)], Gerhard Grübel[(2)], and Werner Press[(1)]

[(1)] Institut Laue-Langevin , BP 156, F-38042 Grenoble (France)

[(2)] ESRF , BP 220, F-38043 Grenoble (France)

[(3)] Experimentelle Physik 1, Universität Dortmund
Otto-Hahn-Str. 4, D-44221 Dortmund (Germany)

[(*)] Corresponding author. Electronic address: seydel@ill.fr

April 25, 2003

Abstract

A dedicated setup comprising an efficient cryogenic device for the in-situ preparation of large surface areas of prototypical organic glass formers in a wide temperature range (170–340K) is presented. This setup provides the necessary temperature and vibrational stability for surface x-ray and neutron scattering experiments including the extremely sensitive technique of x-ray photon correlation spectroscopy (XPCS). XPCS is an emerging method which is made possible by the high coherent photon flux produced by 3rd generation synchrotrons. We demonstrate that microscopic motion at the surface can be studied in a direct way in the liquid and supercooled state using XPCS. In addition, we have used a CCD-detector to record 2-dimensional images of static speckle patterns forming on surfaces in the glassy state.

PACS numbers: 68.03.Kn, 68.15.+e, 61.41.+e, 61.10.-i

1 Introduction

Glasses are characterized by the structural disorder known from liquids but also by microscopic dynamical processes very far from those of a liquid [1]. The transition from a liquid to a glass is characterized by an exponential increase of the viscosity. Little is known about the glass transition at the surface and there has been much debate about possible differences to the bulk transition. The rms roughness and long-range correlations of a liquid surface are essentially determined by thermally activated capillary waves [2, 3, 4, 5]. The common hydrodynamic theory predicts that the high viscosity near the glass transition causes capillary waves at the surface to be overdamped. These waves are expected to gradually freeze due to an exponential increase in the characteristic time τ_0 of their motion [2, 6]. Only recently, experimental tests of these predictions have been achieved by x-ray scattering on surfaces of simple glass formers with bulk properties [7, 8]. In this article we report on the necessary instrumental pre-requisites for these experiments and give a full scope of examples. We mainly focus on the technical aspects, while the physical questions to be resolved and underlying theory are discussed elsewhere, the references being provided in the course of this text.

Diffraction patterns generated with light from a coherent source can show a graininess known as speckle. The speckle pattern is caused by phase shifts of the incident plane wave introduced during the diffraction process by a modulated spatial arrangement of the sample [9, 10]. Since the advent of high brilliance synchrotron x-ray sources it has been possible to observe speckle in x-ray diffraction patterns [11, 12, 13]. Speckle patterns from static surfaces have previously been recorded using a CCD camera to demonstrate the co-

herence properties of the impinging radiation [12]. The time variation of a speckle pattern is related to the dynamics of the sample and x-ray photon correlation spectroscopy (XPCS) has for instance been used to investigate the complex dynamics of colloidal suspensions [14, 15, 16]. These studies apply a transmission geometry and hence are sensitive to bulk dynamics. The XPCS technique is closely related to dynamic light scattering [17, 18, 19], but with the advantage that the smaller wavelength of x-rays allows access to larger momentum transfers (q-vectors) and permits to investigate opaque materials.

When x-rays are incident on a surface below the critical angle for total external reflection the scattered intensity is solely coming from the atoms or molecules in the near-surface region. Scattering of coherent x-rays incident on a surface under grazing angles can therefore be used in a direct and unambiguous way to measure temperature dependent changes in the surface dynamics of a supercooled liquid or glass. In general, the correlation function measured by XPCS is related to the so-called intermediate scattering function $S(q,t)$ [20]. With the lateral length and time scales currently accessible, surface XPCS can thus be applied to measure capillary wave fluctuations with a high resolution in wavevector and time [7, 21, 22]. On highly viscous liquids, the ratio of the viscosity and the surface tension can be determined from XPCS on micrometer length scales [23]. Although on these length scales XPCS and visible light photon correlation spectroscopy (PCS) still compete, the advent of x-ray sources with higher brilliance will make shorter length scales accessible to surface XPCS. The surface sensitivity below the critical angle and the posibility of x-rays to penetrate opaque windows of cryostated sample environments and ultra high vacuum chambers already now renders XPCS superior to PCS.

Further, the very recent discovery of heterodyne mixing effects in surface XPCS experiments [20, 24] may offer a future perspective to achieve even larger wave vector transfers.

In addition to the emerging techniques using x-rays with a high degree of transverse coherence, the well-established scattering experiments measuring the reflectivity and diffuse scattering of "incoherent" x-rays from a surface may be applied. When the x-rays are incident well above the critical angle, the resulting reflected intensity allows for infering on the rms roughness of a surface [4, 5, 25]. The off-specular diffusely scattered intensity then contains information on the lateral correlations of the surface [26]. Such a measurement may therefore be used to determine the roughness of a liquid *in-situ* while it is supercooled and undergoing a glass transition [8]. Hence, it may be tested if the long-range correlations which are characteristic for capillary waves on a liquid surface remain unchanged or are altered with the rising viscosity.

For these types of experiments large surfaces of prototypical glass forming substances have to be prepared and cooled homogeneously through the glass transition. The samples have to be sufficiently deep to be free of substrate effects, and crystallization has to be circumvented. Furthermore, the setup has to provide the possibility to stabilize any desired temperature over several hours to better than 0.02 K. Our sample environment fulfills these requirements, and in the following section 2 we will describe it in detail. Section 3 contains technical notes on the temperature-dependent surface characterization by (incoherent) x-ray reflectivity and diffuse scattering measurements. In section 4, the experimental setup and examples of x-ray photon correlation spectroscopy measurements will be presented. Two-dimensional images of

speckle patterns from fluctuating and static surfaces which have been recorded with a CCD detector will be discussed in detail in section 5. A brief conclusion is presented in section 6.

2 The sample environment

For the in-situ experiments described in this article a dedicated sample environment has been developed [27]. The samples with macroscopic thickness are prepared in a trough of 140 mm diameter and approximately 4 mm depth inside an aluminum sample chamber (Fig.1). The large diameter of the sample ensures that the illuminated surface is not affected by a meniscus of the liquid at the borders of the sample container and that a large footprint of the incident beam under grazing angles fits on the sample. The trough is filled to approximately 0.1mm above its upper rim, and a meniscus is created. This is possible due to the finite surface tension of the liquid. Therefore, the incident beam does not hit the upper rim of the trough even at zero incident angle. The sample chamber and the trough within are machined out of a single piece of aluminum to achieve a good thermal conductivity and to allow for a thorough cleaning. The sample chamber is covered with a *Viton*-sealed top lid that can be removed for the cleaning of the trough. The filling is done through an inlet device to reduce the exposure of the sample to the outside air to a minimum.

After filling the trough with the liquid, the sample chamber is evacuated to approx. 10 mbar in order to reduce the background scattering from the gas and then hermetically sealed. The pressure inside the sample chamber can be monitored by a miniature sensor. The remaining pressure above the sample is

essentially the vapor pressure of the liquid. This may yield different levels of the measured background signal in reflectivity experiments since it is not possible to control this temperature-dependent parameter. The background level is important in x-ray reflectivity measurements from bulk liquid surfaces since isotropic bulk scattering dominates the scattering for large wave-vector transfers [28] and isotropic bulk scattering cannot be distinguished from isotropic background scattering arising from the remaining vapor. In the case of reflectivity measurements the surface signal has to be determined by subtracting the separately measured background. However, in the case of scattering experiments with the angle of incidence being always smaller than the critical angle, the background scattering from the bulk is neglectible.

A vacuum ($p < 10^{-5}$ mbar) is maintained in an outer aluminum cell surrounding the sample chamber for thermal insulation. For this purpose, a turbomolecular pump is connected to the outer cell via a flexible metal tube. It turned out that even speckle imaging measurements are not hampered by vibrations while the pump is running. High-frequency vibrations are apparently effectively reduced by the large mass (approximately 15 kg) of the cell (i.e. the sample chamber plus the outer cell) and its rigid mounting on the diffractometer. An active vibration damping system is also not necessary, since low-frequency vibrations which may be induced from outside do not affect highly viscous liquids. Such problems may, however, occur for low viscosity liquids such as water.

The x-ray beam penetrates both the inner and outer cell walls through Kapton foil windows (thickness approx. $25\,\mu$m per layer). For the XPCS experiments, the outer cell surrounding the sample chamber can be directly

attached with a vacuum flange to the detector flight tube of the diffractometer. This reduces the number of Kapton foil windows in the beam, which might affect the degree of coherence of the radiation.

In order to record the temperature of the sample two ceramics-coated platinum resistor (Pt100) sensors are dipped into the sample approximately 100 mm apart from each other on opposite sides of the beam footprint.

The cooling of the sample is accomplished with a constant flow of liquid nitrogen evaporating in a heat exchanger underneath the sample chamber. The heat exchanger has the shape of a hollow disk of 10 mm thickness and a diameter matching that of the sample chamber. The brass disk has an empty volume of approximately 53 cm^3 for the evaporation of the liquid nitrogen. Its fabrication requires the so-called hard soldering of its components to ensure a sufficient thermal stress resistance. The disk stands with its bottom face on small teflon pads in the outer aluminum cell to allow for an evacuated volume for thermal insulation. The liquid nitrogen is fed through a narrow (5 mm outer diameter) brass inlet tube from outside the outer cell, and the exhaust is accomplished by an equivalent outlet tube. The brass tubes are in contact with the bottom wall of the outer cell solely via *Viton* vacuum seals in order to minimize the thermal loss. The connection between the brass inlet and outlet and, respectiviely, the nitrogen dewar and exhaust gas pump is accomplished by flexible Teflon tubes.

The sample chamber is attached to the heat exchanger using a bayonet fixing ensuring a good thermal contact to the disk at both its top face and side. The thermal contact is further enhanced by an adequate heat sink compound (e.g. *Apiezon N*). The nitrogen flow rate is set by a control valve in the exhaust

gas stream. The best stability of the flow rate can be achieved with a mass flow controller (adjustable flow rate 0 to 30 l/min.). The liquid nitrogen dewar is kept at nearly ambient pressure and a membrane pump in the exhaust gas tube generates the flow. The heating of the sample is achieved with an electric resistor sandwiched into Kapton foil (*Minco Products, Minneapolis, MN, USA*) underneath the heat exchanger. The resistor is connected to a Lakeshore temperature controller allowing for a maximum heating power of 45 W. In addition, the top lid of the sample chamber can be independently heated. A temperature stability better than 0.02 K is achieved in a temperature range from 170 K to 340 K. A third Pt100 sensor is used to separately monitor the temperature of the heat exchanger. The good stability of the temperature over a long time is in particular required for the XPCS experiments, as instabilities may introduce parasitic time correlations in the measurements.

The nitrogen flow rate for a cooling rate of about 1.5 K/min. amounts to approximately 20 l/min. of gaseous nitrogen (measured at room temperature and ambient pressure) in the exhaust gas stream. Only taking into account the heat exchange due to the evaporation of the nitrogen, a heat transfer of about 5×10^3 J/min. can be estimated. The total mass of the sample chamber (i.e. the inner cell alone) is nearly 1.5 kg. Assuming the heat capacity $c_{Al} \approx 900$ J/kgK (at $T = 300$ K) of aluminum to describe the total heat capacity of the chamber, about 2×10^3 J/min. is therefore exchanged. Thus, the cooling device is highly efficient under the difficult geometrical restrictions (large sample surface). The sample may be easily held at $T = -90°$ C for more than 24 h, which has proven to be particularly useful for neutron scattering experiments with long counting times.

3 X-ray reflectivity and diffuse scattering

X-ray reflectivity measurements using the sample chamber described in the previous section have already been published in Ref.[8]. Here we add some comments on the technical aspects for performing such a type of experiment.

For liquid surfaces, a particular experimental difficulty in measuring the reflectivity arises from the necessity to keep the sample surface horizontal. The incident beam has therefore to be inclined within a large angular range and with a precision better than one mrad. Using an x-ray tube source, this may be achieved by rotating the source around the sample or, in the case of a rotating anode, rather by making use of the large divergence of the emitted radiation through the rotation of a pair of slits around the anode [27]. Recently, liquid surface diffractometers with x-ray tube sources have become commercially available (D8 by *Bruker-AXS*), and additionally a number of individually designed instruments exists at rotating anodes [27]. However, in order to determine the roughnesses of comparatively smooth liquid surfaces with high precision, the high flux of a synchrotron radiation source is required, since the measured reflectivity deviates from the Fresnel reflectivity of an ideally smooth surface only at large q_z. Only a few diffractometers at synchrotrons worldwide are optimized for this purpose, one of them being the Harvard/BNL liquid surface diffractometer at the National Sychrotron Light Source beamline X22B at Brookhaven National Laboratory (see e.g. [4] and references therein).

The rms roughness measured from a free surface of a deep liquid depends on the experimental resolution through a logarithmic term when measured by x-ray reflectivity [25]. A detailed discussion of resolution effects in surface x-ray scattering experiments can be found in Ref.[29]. At diffractometers using

x-ray tube sources it is technically less challenging to achieve a good angular resolution than at diffractometers using synchrotron radiation. This is due to simple mechanical reasons, because fewer movements are required to tilt the beam at tube sources. For instance, at the liquid surface diffractometer in the Physics Department at the University of Kiel (Germany) using a rotating anode x-ray source, an angular resolution of approximately 0.35 mrad has been achieved by the special design of the instrument [27]. To illustrate this, an example of a measurement at this instrument is shown in the figure 2. The diffuse scattering from a glycerol surface at room temperature around the specular peak is shown in a log-log plot as a function of the lateral wave vector transfer q_x at a fixed $q_z \equiv 0.07\,\text{Å}^{-1}$ (symbols in the figure). Open symbols denote data taken at $q_x < 0$ after the transformation $q_x \longrightarrow |q_x|$. The agreement between the data denoted by open and filled symbols, respectively, is thus an indication of the qualtiy of the alignment of the diffractometer. The width of the specular peak at $q_x = 0$ is essentially given by the experimental resolution. The resolution at $q_z \equiv 0.07\,\text{Å}^{-1}$ has been estimated from the direct beam profile of the instrument according to $q_x = \frac{1}{2}\alpha_f q_z$, where α_f is the detector take-off angle (dashed line in the figure). The solid line indicates a fit to the capillary waves model [5].

4 X-ray photon correlation spectroscopy

Whether the capillary wave modes are propagating, overdamped or frozen-in as a function of temperature and wavevector cannot be distinguished by the conventional x-ray scattering experiments that have been briefly mentioned in

the previous section. Coherent x-rays, however, may be used to determine the dynamics in a direct way [30].

Using the setup described in section 2, we have performed XPCS measurements on glycerol and different polymer surfaces at the ID10 Troïka A beamline of the ESRF with 8 keV radiation (wavelength $\lambda = 1.548$ Å) originating from three insertion devices. The experiment on glycerol has been reported in detail in Ref.[7]. In this section we add some technical aspects. To tilt the incident beam down from the storage ring plane, both the Si(111) monochromator and a Platinum mirror which was located downstream from the monochromator were aligned to provide adequate angular offsets (see Fig.3). The angle of incidence on the sample was kept constant at about 0.08° well below the critical angle for total reflection. The envanescent wave penetrates in this case only the topmost ~ 80Å. The alignment of the incident angle was done by making use of the relative rotating movement of the platinum mirror, the absolute mirror to sample and sample to detector distances, the relative sample height movement and the liquid sample surface which can be assumed to be perfectly horizontal.

The wavelength bandpass from the Si(111) monochromator is $\Delta\lambda/\lambda \approx 10^{-4}$ yielding a longitudinal coherence length $\xi_l = \lambda^2/\Delta\lambda$ of about 1 μm. A pinhole with a diameter of 12 μm was mounted 278 mm upstream from the sample in order to obtain a collimated and (partially) coherent beam. The intensity behind the pinhole amounts to approx. $2 \cdot 10^9$ photons/second. The typical transverse coherence length at the pinhole is 10 μm. A guard slit in front of the sample was used to suppress the Fraunhofer diffraction from the pinhole. The data were collected with a NaI scintillation counter at a distance 2368 mm

downstream from the sample. An aperture with an adjustable size of 5 μm–100 μm was chosen in front of the detector. The adjustable size allowed to balance between a high speckle contrast (small aperture) and a high flux by averaging over several speckles (large aperture) [31]. The time-autocorrelation functions were recorded with a digital ALV5000/E correlator.

The scattered radiation was detected under different exit angles α_f within the scattering plane. Hence the lateral and perpendicular components of the wavevector transfer, q_x and q_z, are given by $q_x = (2\pi/\lambda)(\cos\alpha_f - \cos\alpha_i)$ and $q_z = (2\pi/\lambda)(\sin\alpha_f + \sin\alpha_i)$. From the q_x-value the respective lateral length scale x_0 that is probed may be obtained by $x_0 = 2\pi/q_x$. The error in the determination of x_0 is related to the error in the measurement of the flight path lengths which is a few millimeters yielding a relative error on the order of 10^{-3}.

Surface dynamics can be measured in a photon correlation spectroscopy experiment by evaluating the normalized time-autocorrelation function $G(\tau) = \langle I(t+\tau)I(t)\rangle_t / \langle I(t)\rangle_t^2$ where $I(t)$ is the observed intensity in a detector [17, 18, 19]. We found that our data can be well described by the exponential form

$$G(\tau) = g_0 \exp(-\tau/\tau_0) + 1 \,, \tag{1}$$

with $0 \leq g_0 \leq 1$ and a time constant τ_0. The constant g_0, also denoted as contrast, depends on the degree of coherence of the incident beam and the degree of ensemble averaging for the incident and scattered beam [31]. Equation 1 describes the measured correlation in the case of overdamped capillary waves [6, 18]. Very recent further experiments and calculations have revealed that a heterodyne mixing of the diffusely scattered signal and the specular reflected beam takes place [24, 20]. However, the effect on the determination of the time

constants of overdamped waves is small.

In the figure 4 two examples of correlation functions that have been obtained from a surface of glycerol are given. In the first example (Fig.4 (a)), a particularly high contrast $C = (67.6 \pm 0.2)\%$ has been achieved. The lateral length scale probed was $x_0 = 90\,\mu$m and the opening of the exit aperture in front of the detector was set to $5\,\mu\text{m}\times 15\,\mu\text{m}$ ($v \times h$). The temperature of the glycerol sample was $T = 265.7\,\text{K}$. The fit of Eq. (1) to the data (solid line in Fig. 4) yields the relaxation rate $\tau_0^{-1} = (0.253 \pm 0.01)\,\text{ms}^{-1}$ and hence $\tau_0 = 3.95\,\text{ms}$, and the contrast quoted above. The total correlation time for this measurement was nearly 15 minutes and the average count rate in the detector approximately 100 Hz. In the second example (Fig.4 (b)), a shorter lateral length scale $x_0 = 5.6\,\mu$m was probed. The temperature of the glycerol sample was $T = 234.15\,\text{K}$. The aperture in front of the detector was set to $50\,\mu\text{m}\times 300\,\mu\text{m}$ ($v \times h$). Here, the fit yields $C = 2.52\,\%$ and $\tau_0 = 106.38\,\text{ms}$. The total correlation time for the second example was 20 minutes and the average count rate in the detector approximately 150 Hz.

The maximum achievable contrast is partly determined by geometrical conditions [31], and it turns out that with a fixed slit setting it decreases with rising lateral wave vector transfer q_x. To measure a correlation function, a minimum count rate depending on the time scale of the fluctuation to be detected and other factors such as the stability of the setup is required, thereby limiting the accessible q_x-range. Up to now, the minimum length scale that can be tested on our samples is therefore on the order of one micrometer. We note that a correlation function from our highly viscous liquid samples can be taken only after waiting for the whole setup to stabilize at a given temperature

T, which is typically at least one hour and strongly depends on T.

Improvements of the storage ring current and the undulators will increase the available flux incident on the sample in the future. Furthermore, a less monochromatic incident beam may be considered, as a slightly reduced longitudinal coherence can be allowed in the grazing incidence geometry. In addition, the stability of our experimental setup might still be further improved. Thus, we envisage that shorter lateral length scales will be achievable in the future. A lower limit for the minimum accessible time scale is given by the time structure induced by the electron bunches in the storage ring. At the ESRF this time scale is a few nanoseconds in uniform filling mode. Experiments detecting motion on a time scale of approximately 50 ns have already been performed [32] using a faster avalanche photodiode (APD) detector instead of the NaI.

It appears that in our XPCS experiment with the angle of incidence of the x-ray beam being allways smaller than the critical angle of total external reflection, there are only little difficulties arising from beam damage. By scattering from surfaces of deep liquids, damage caused by substrate photoelectrons is circumvented. We have changed the illuminated spot on our samples occasionally and observed only slight changes in the maximum achievable contrast.

5 2-dimensional detection with a CCD

The direct visualization of a speckle pattern using a two-dimensional CCD camera gives additional information related to the spacial shape of the speckles and their q-dependence [31]. Furthermore, the CCD experiment can provide a proof of a surface which is completely frozen-in on a time scale of at least

several hours at a sufficiently low temperature. In the case of our setup, a time scale that large is not suitable for XPCS with a point detector. By contrast, the CCD-experiment using a 2-dimensional detector is well-suited to study time-averages, as we discuss in this section. The CCD-detector can as well be used for XPCS experiments to study slow dynamics, as has been shown by Kim et al. [33] on thin polymer films on silicon substrates. For a detailed discussion of using a CCD to perform XPCS we refer to Lumma et al. [34].

The same beamline setup as described in the previous section was used to direct the monochromatic and partially coherent beam downwards to be incident on a horizontal glycerol surface with an incidence angle $\alpha_i = 0.08^o$. The radiation scattered from the surface was detected using a direct illumination CCD camera from Princeton Instruments with a pixel size of $22.5 \times 22.5\,\mu\mathrm{m}^2$. The CCD camera was placed instead of the NaI detector and detector aperture described in section 4 to record the two-dimensional off-specular diffuse scattering image from the surface. The two coordinates of the CCD image thus correspond to the lateral components (q_x, q_y) of the wavevector transfer within and perpendicular to the scattering plane.

In the example presented here, the slowing down of surface dynamics is directly visualized by the CCD images obtained at two different temperatures of a glycerol sample (Fig.5). In the figure, the intensities in the pixels of the CCD camera along the in-plane diffuse rod (i.e. along q_x with $q_y \equiv 0$) are given for (a) $T = -34.3^oC$ and (b) $T = -80.0^oC$. These intensities have been obtained by adding the indicated number of frames, i.e. consecutive exposures of the CCD. Each frame has been exposed for 50 ms for the measurement at $T = -34.3^oC$, respectively for 20 ms for the measurement at -80.0^oC.

Between each two exposures a few seconds elapsed for the read-out of the CCD. Hence, the total integration time to record the several hundred frames per sample was on the order of one hour. The data are normalized to equal total intensity and shifted for clarity along the intensity axis in the plot. Above the plotted intensities along q_x, the corresponding two-dimensional CCD images for the respective maximum number of frames are shown. The rod-like shape of the scattered intensity [31] and the speckle pattern in the low-temperature case become apparent.

We note that only two orders of magnitude in intensity difference may be detected at once along the CCD that we have used. This is related to the large number of charges created at once in a CCD pixel by a single x-ray photon. Furthermore, the quantum efficiency of a single CCD pixel is limited to approximately 30%. In addition, a significant intensity was present in the dark images. Therefore, when only a few frames are added, both the images from the low-temperature and the high-temperature sample show statistical noise which might be mistaken as speckle (Fig.5). However, when a few hundred frames are added, the data from the frozen-in sample may be clearly identified as a static speckle pattern, whereas summing the frames from the fluctuating sample results in a smooth image. The low-temperature sample is therefore static on a time scale of at least one hour over which the CCD frames have been integrated. This interpretation is further supported by the strong intensity modulation along q_x at small q_x in the case of the static sample. Here, statistical noise would have the opposite effect of strongly modulating at large q_x where the absolute intensity is low.

For comparison, CCD images have also been taken from a silicon wafer

which was placed instead of the glycerol within the sample cell (Fig.6). The wafer serves as a static reference sample. When illuminated through the usual 12 μm pinhole, a speckle pattern appears in the diffuse scattering (Fig.6 (a)). We note that the wafer may not be as perfectly aligned as the liquid and frozen-in glycerol surfaces presumably because it is slighly bent due to its large size. The silicon wafer has also been used to verify that when deliberately destroying the coherence of the incident beam by opening the pinhole to 100 μm, a smooth scattering pattern results similar to the pattern from the fluctuating sample (Fig.6 (b)).

6 Outlook

We have presented an experimental device which allows for a wide variety of *in-situ* surface investigations with x-ray scattering methods. In particular, the device is adapted to the extremely sensitive XPCS experiments. The device may as well be used for experiments with neutrons, since the thin (0.25 μm each) Kapton foil windows cause only negligible absorption even for cold neutrons. In addition, the experimental setup has already been shown to be equally suitable for glycerol and prototypical polymer glasses. In future experiments, it may be possible to test predictions related to the surface dynamics, viscosity and surface tension of polymers using XPCS in the described setup.

It turns out from the reflectivity measurements that the supercooled glycerol surfaces are surprisingly smooth with an rms roughness of approx. 2 Å in the glassy state. The sample preparation causes no imperfections on the surface even in the frozen-in state provided that adequate cooling rates to cir-

cumvent crystallization are respected. Speckle imaging with the CCD camera provides proof of a surface that is completely static. The main focus on future developments will be to access shorter lateral length scales in XPCS. So far, the limits have certainly not yet been reached.

Acknowledgements

This work was supported by the 'Deutsche Forschungsgemeinschaft' (project numbers Pr325/9-1,2,3, Pr325/12-1 and Pr325/14-1). The measurements with coherent x-rays were carried out at the Troïka beamline ID10A of the European Synchrotron Radiation Facility (ESRF).

References

[1] W. Götze and L. Sjögren, *Rep. Prog. Phys.* **55**, 241 (1992).

[2] J. Jäckle, K. Kawasaki; J. Phys.: Condens. Matter **7**, 4351 (1995).

[3] U-Ser Jeng, Levon Esibov, Lowell Crow and Albert Steyerl; J. Phys.: Condens. Matter **10**, 4955 (1998).

[4] A. Braslau, P.S. Pershan, G. Swislow, B.M. Ocko, J. Als-Nielsen; Phys. Rev. A **38**, 2457 (1988).

[5] M.K. Sanyal, S.K. Sinha, K.G. Huang, B.M. Ocko; Phys. Rev. Lett. **66**, 628 (1991).

[6] V.G. Levich; *Physicochemical Hydrodynamics*, Prentice-Hall, Englewood Cliffs NJ (1962).

[7] T. Seydel, A. Madsen, M. Tolan, G. Grübel, W. Press; Phys. Rev. B **63**, 073409 (2001).

[8] T. Seydel, M. Tolan, B.M. Ocko, O.H. Seeck, R. Weber, E. DiMasi and W. Press; Phys. Rev. B **65**, 184207 (2002).

[9] J.C. Dainty(editor), *Laser Speckle and Related Phenomena*, Springer-Verlag, Berlin (1984).

[10] K.F. Ludwig Jr.; *Phys. Rev. Lett.* **61**, 1526 (1988).

[11] M. Sutton, S.G.J. Mochrie, T. Greytak, S.E. Nagler, L.E. Berman, G.A. Held, and G.B. Stephenson; *Nature* **352**, 608 (1991).

[12] Z.H. Cai, B. Lai, W.B. Yun, I. McNulty, K.G. Huang, and T.P. Russell; *Phys. Rev. Lett.* **73**, 82 (1994).

[13] D.L. Abernathy, G. Grübel, S. Brauer, I. McNulty, G.B. Stephenson, S.G.J. Mochrie, A.R. Sandy, N. Mulders, M. Sutton; *J. Sync. Rad.* **5**, 37 (1998).

[14] T. Thurn-Albrecht, W. Steffen, A. Patkowski, G. Meier, E.W. Fischer, G. Grübel, and D.L. Abernathy; *Phys. Rev. Lett.* **77**, 5437 (1996).

[15] O.K.C. Tsui and S.G.J. Mochrie, *Phys. Rev. E.* **57**, 2030 (1998).

[16] G. Grübel, D.L. Abernathy, D.O. Riese, W.L. Vos, G.H. Wegdam, *J. Appl. Cryst.* **33**, 424 (2000).

[17] B. Berne and R. Pecora, *Dynamic Light Scattering*, Wiley-Interscience, New York (1975).

[18] D. Byrne and J.C. Earnshaw, *J.Phys.D:Appl.Phys.* **12**, 1133 (1979).

[19] D. Langevin (Editor); *Light Scattering by Liquid Surfaces and Complementary Techniques*, Marcel Dekker, New York (1992).

[20] A. Madsen, T. Seydel, M. Sprung, C. Gutt, M. Tolan, G. Grübel; submitted to Phys. Rev. Lett.

[21] Fast density fluctuations (e.g. elastic shear modes) are, however, beyond the accessible time window.

[22] A. Madsen, J. Als-Nielsen, G. Grübel; Phys.Rev.Lett.**90**, 085701 (2003).

[23] In the case of propagating capillary waves, the surface tension and the viscosity may be obtained independently. In the case of overdamped waves on very viscous liquids, only the ratio of these quantities can be obtained. Since the capillary waves at the surface are a result of fluctuations in the bulk liquid, the viscosity as determined from XPCS is not necessarily the viscosity at the surface.

[24] C. Gutt, T. Ghaderi, V. Chamard, A. Madsen, T. Seydel, M. Tolan, M. Sprung, G. Grübel, S.K. Sinha; submitted to Phys. Rev. Lett.

[25] B.M. Ocko, X.Z. Wu, E.B. Sirota, S.K. Sinha, M. Deutsch; Phys. Rev. Lett. **72**, 242 (1994).

[26] S.K. Sinha, E.B. Sirota, S. Garoff and H.B. Stanley; Phys. Rev. B **38**, 2297 (1988).

[27] T. Seydel; PhD thesis, University of Kiel, Germany, (2000).

[28] C. Fradin, A. Braslau, D. Luzet, D. Smilgies, M. Alba, M. Boudet, K. Mecke, J. Daillant; Nature (London) **403**, 871 (2000).

[29] D. Sentenac, A.N. Shalaginov, A. Fera, W.H. de Jeu; J.Appl.Cryst. **33**, 130 (2000).

[30] M. Tolan, T. Seydel, A. Madsen, G. Grübel, W. Press and S.K. Sinha; Appl.Surf.Sci. **182**, 236 (2001).

[31] A. Madsen, G. Grübel, T. Seydel and M. Tolan, to be published.

[32] I. Sikharulidze, I.P. Dolbnya, A. Fera, A. Madsen, B.I. Ostrovskii, and W.H. de Jeu; Phys.Rev.Lett. **88**, 115503 (2002).

[33] H. Kim, A. Rühm, L.B. Lurio, J.K. Basu, J. Lal, D. Lumma, S.G.J. Mochrie, S.K. Sinha; Phys.Rev.Lett. **90**, 068302 (2003).

[34] D. Lumma, L.B. Lurio, S.G.J. Mochrie; Rev.Sci.Inst. **71**, 3274 (2000).

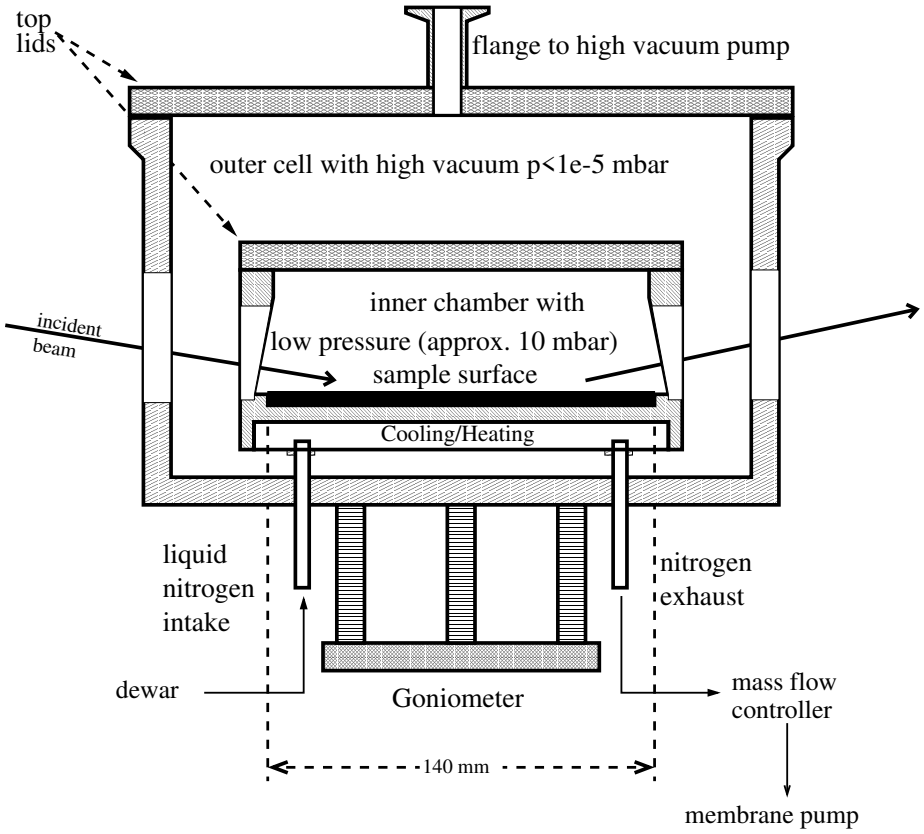

Figure 1: Sketch of the sample environment (side view, drawn to scale) consisting of an outer cell evacuated to approximately 10^{-5} mbar for thermal insulation and an inner chamber which contains the trough for the sample. Both the inner chamber and outer cell have a cylindrical symmetry along the vertical axis. The inner chamber is mounted on the heat exchanger (see text for details).

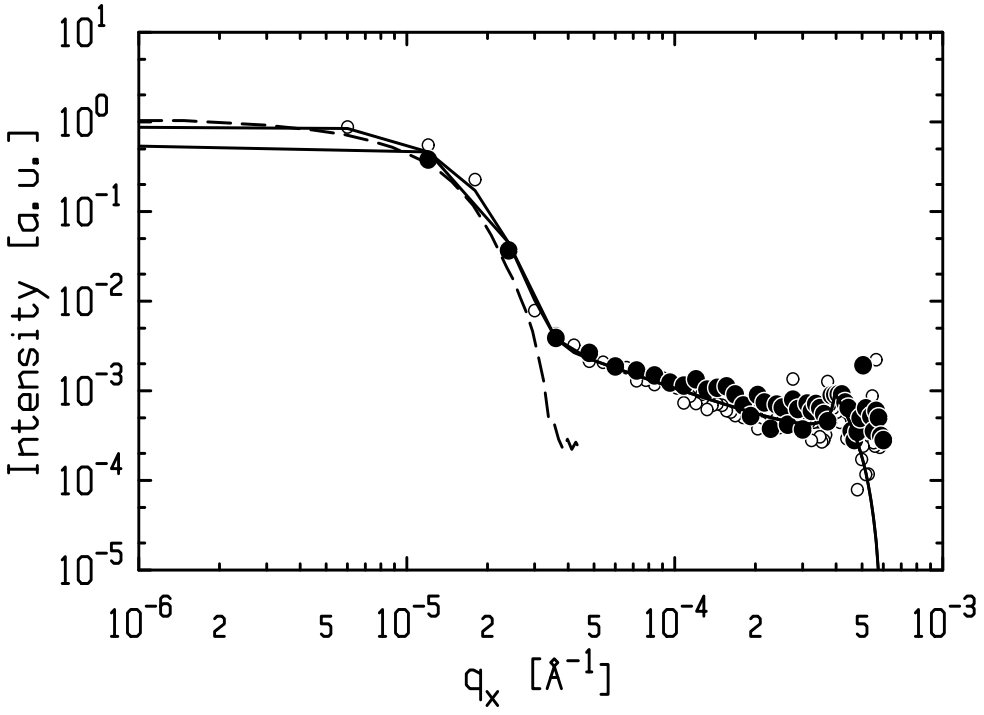

Figure 2: Scattered intensity from a glycerol surface at ambient temperature as a function of the lateral wave vector transfer in the scattering plane q_x while q_z was kept constant at q_z =0.07Å^{-1} (symbols). The data were taken at a liquid surface diffractometer using a rotating anode x-ray source. A constant background has been subtracted, and the data have been corrected for the variation of the illuminated and detected spot size on the sample as a function of incidence and take-off angle. The dashed line is an estimation of the resolution function from the measured direct beam profile according to $q_x = \frac{1}{2}\alpha_f q_z$, where α_f is the detector take-off angle. The solid line is a fit to the standard capillary wave model. (See further explanations in the text.)

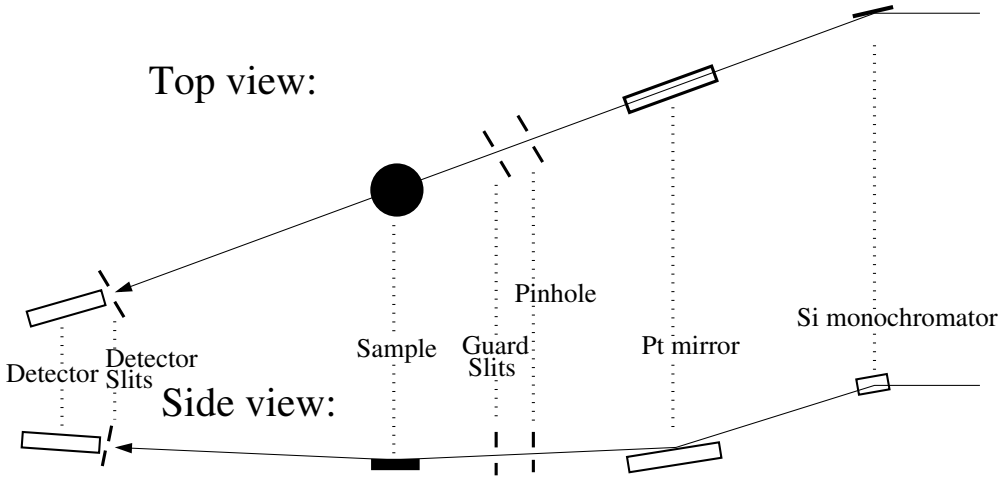

Figure 3: Sketch of the setup for the XPCS experiment (not drawn to scale). The Si111 monochromator is tilted to bring the incident beam downwards at a fixed angle. The downstream platinum mirror with its reflecting surface facing upwards both suppresses the higher order reflections from the monochromator and is used to align the incident angle (see text for details).

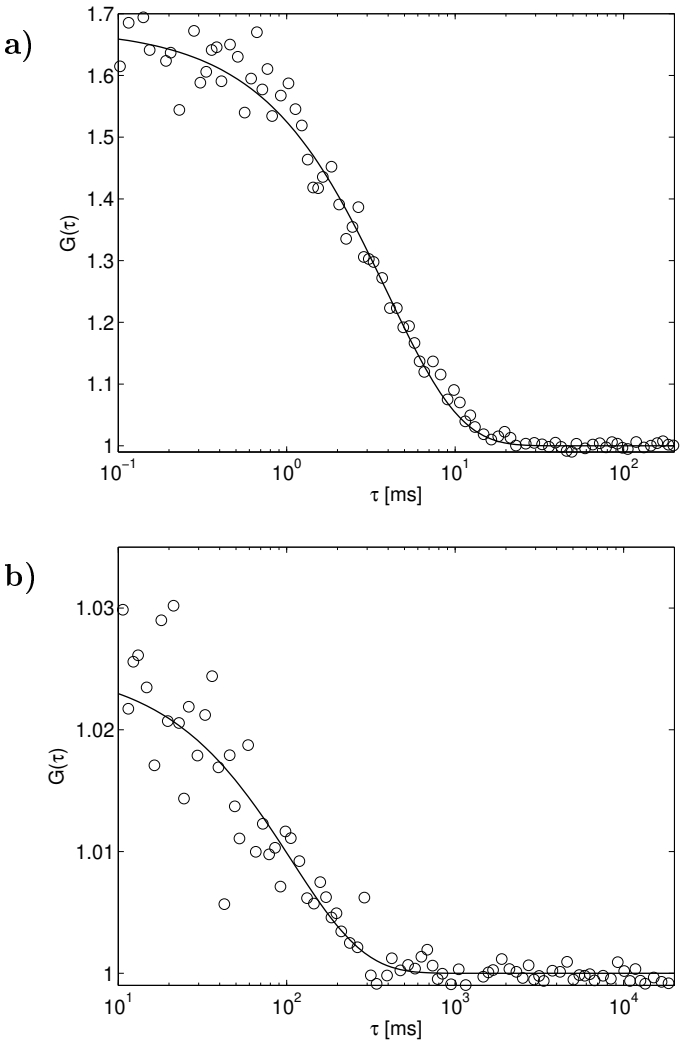

Figure 4: Intensity-intensity correlation functions $G(\tau)$ (open circles) from a glycerol surface at different temperatures and length scales. The solid lines are fits according to $G(\tau) = g_0 \exp(-\tau/\tau_0) + 1$ from which the two parameters g_0 (contrast) and τ_0 (time constant of overdamped capillary waves) are obtained. (a) The temperature is $T = 265.7\,\mathrm{K}$ and the lateral length scale that was probed is $l_x = 90\,\mu\mathrm{m}$. (b) $T = 234.15\,\mathrm{K}$ and $l_x = 5.6\,\mu\mathrm{m}$.

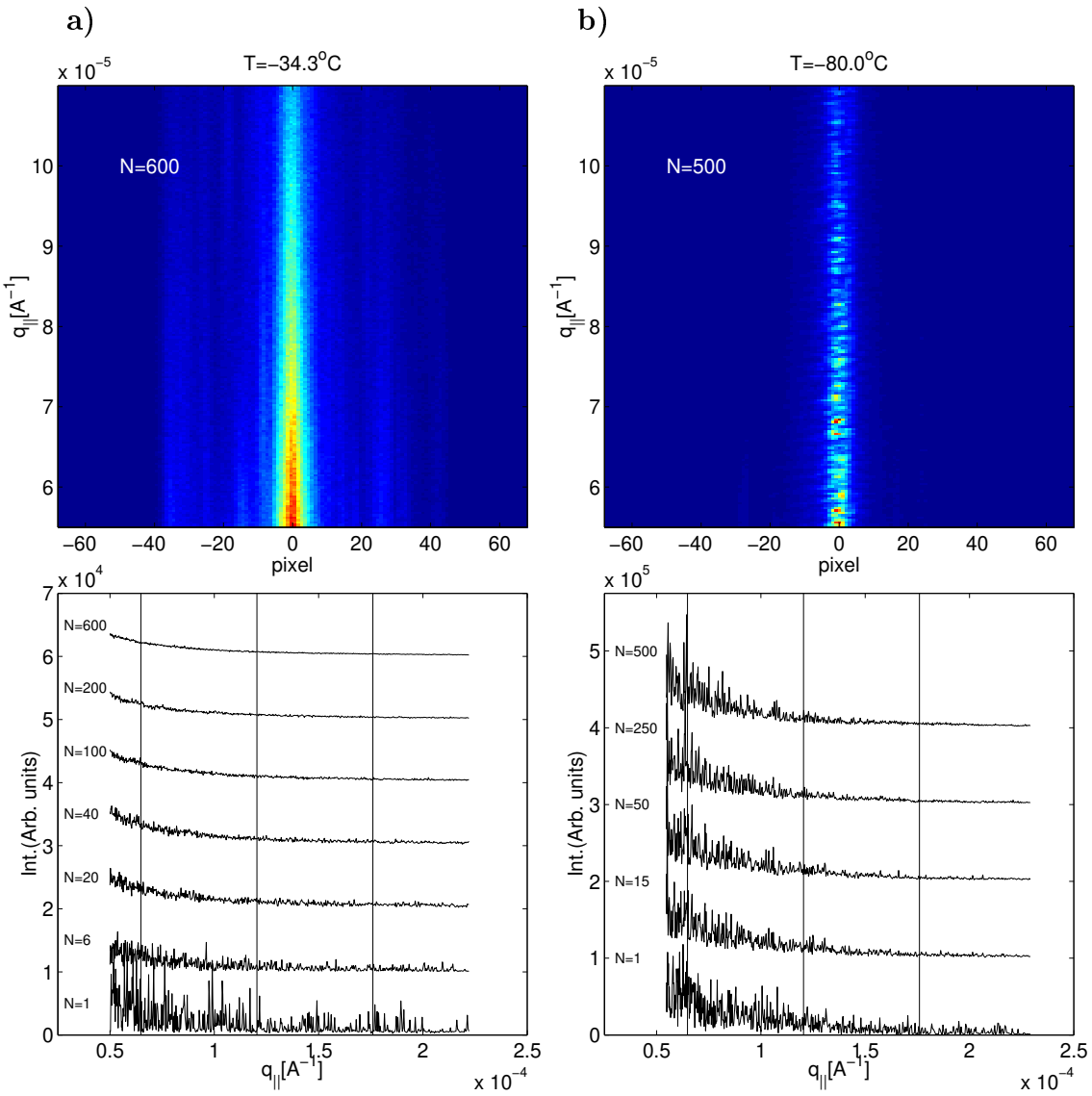

Figure 5: CCD data of a glycerol surface at (a) $T = -34.3^oC$, (b) $T = -80.0^oC$. The intensity in the CCD pixels corresponding to the scattering plane is plotted for a rising number N of added frames (i.e. consecutive exposures of the CCD camera) with (a) 0.05s (b) 0.02s exposure each. The data have been normalized to equal integrated intensity after subtraction of a constant background and then shifted for clarity along the intensity axis. Above, the 2-dimensional CCD images corresponding to the respective maximum number of frames are shown.

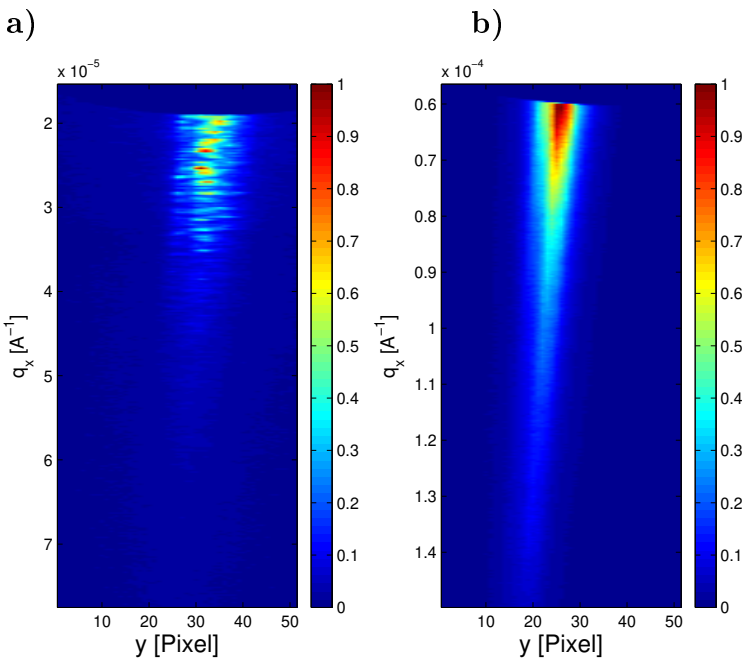

Figure 6: 2-dimensional CCD images of a Silicon wafer surface at ambient temperature using the same experimental geometry as in figure 5. The wafer has been illuminated through (a) the 12 μm pinhole and (b) the 100 μm pinhole. In both cases, 1000 frames with 20 ms exposure time each have been added. In the case of the large pinhole, an aluminum attenuator has been placed in the incident beam. A constant background has been subtracted. It becomes apparent that the incoherent illumination results in a smooth diffuse scattering pattern. The shade at the lowest q_x results from a beamstop for the specular reflection.